Pergamon

Int. J. Solids Structures Vol. 33, No. 9, pp. 1229–1242, 1996

0020–7683/96 $15.00 + .00

0020–7683(95)00096–8

ANALYTICAL MODEL OF FATIGUE CRACK GROWTH RETARDATION DUE TO OVERLOADING

V. V. BOLOTIN and V. L. LEBEDEV
Moscow Power Engineering Institute/Technical University, 111250 Moscow, Russia

(*Received* 5 *December* 1994)

Abstract—A model is suggested to describe the influence of overloading on the fatigue crack propagation process. The model includes three factors that can affect significantly the crack growth rate: the increasing of the material resistance to crack growth due to the crack tip blunting; the residual stress field in the process zone affecting the threshold of microdamage accumulation; the change of microstructural properties close to the new-blunted crack tip that changes the initial conditions of the microdamage accumulation process. It is shown that the joint account of two or three listed factors adequately explains the crack growth retardation due to overloading.

1. INTRODUCTION

Depending on the level of cyclic stresses, on the contribution of plastic deformations and on the total cycle number until the final fatigue fracture, two kinds of fatigue are distinguished: classical (high-cycle) fatigue and low-cycle fatigue. Although each fatigue crack appears to be a very strong stress concentrator producing plastic deformations near the tip, most fatigue phenomena can be described in the framework of the linear fracture mechanics, i.e. considering a cracked body as linear elastic until the final fracture, with the only difference that microdamage near the crack tips is to be taken into account as well as its influence on the material properties (in the first line—on the specific work of fracture). Such an approach was developed by Bolotin (1983, 1985, 1989, 1990).

If the level of loading is comparatively high, plastic deformations and accompanying effects cannot be neglected. In particular, plastic deformations are to be taken into account to describe the effects of overloading on the crack growth rate and the total fatigue life. In fact, most of the factors involved in this phenomena are characteristic for the low-cycle fatigue. In this paper we try to develop an analytical approach to describe the overloading effects. This approach is based on the well-known thin plastic zone model by Leonov–Panasyuk–Dugdale (Liebowitz, 1968; Hutchinson, 1979; Pluvinage, 1989). Bolotin (1987) complemented this model with the microdamage accumulation process affecting the characteristic parameters of the material and developed a model of the low-cycle fatigue crack growth.

According to the theory of fatigue crack growth, a cracked body under loading is considered as a mechanical system with unilateral (due to the irreversibility of cracks) constraints. Two groups of generalized coordinates are introduced: the conventional, Lagrangian coordinates describing the displacement field in the body and the generalized coordinates that were named by Bolotin (1983, 1989), in honor of Griffith, Griffithian coordinates. The latters are needed to describe the position, shape and size of cracks and crack-like defects. Later on, for brevity we say of L- and G-coordinates, respectively. For simplification only quasistatic loading and quasistatic crack behavior will be considered. Under these conditions the response of a cracked body to loading can be analyzed in the framework of the principle of virtual work for systems with unilateral constraints.

Let all the G-coordinates $a_1, \ldots, a_m$ be chosen in such a way that their variations satisfy conditions

$$\delta a_j \geqslant 0, \quad j = 1, \ldots, m. \tag{1}$$

The principle of virtual work can be written as

$$\delta A = \delta_L A + \delta_G A \leqslant 0 \tag{2}$$

where $\delta_L A$ and $\delta_G A$ are the amounts of virtual work produced on L- and G-variations, respectively. If in every time moment the system is in equilibrium with respect to L-coordinates, and all constraints put on L-coordinates are bilateral, eqn (2) takes the form

$$\delta_G A \leqslant 0. \tag{3}$$

Depending on the properties of the virtual work $\delta_G A$, the states of a cracked body under loading can be classified as follows. A state of the system is named a sub-equilibrium state if $\delta_G A < 0$ for all admissible $\delta a_j > 0$. If $\delta_G A = 0$ with respect to a part of G-coordinates and $\delta_G A < 0$ for all the remaining coordinates, the state is named an equilibrium state (with respect to the mentioned part of coordinates). The equilibrium states can be stable, unstable or neutral depending on the property of the following terms in the development of the virtual work into series with respect to δa. At last, a state of the system is named a non-equilibrium state when at least one G-variation exists such that $\delta_G A > 0$. The non-equilibrium states are, evidently, unstable.

With the application to a single-parameter crack with the G-coordinate a, the virtual work $\delta_G A$ can be presented in the form

$$\delta_G A = G\delta a - \Gamma\delta a, \tag{4}$$

where G is the active (driving) generalized force. In simple situations, for example, in the framework of the linear fracture mechanics, G-coordinate coincides with one of the well-known generalized forces, say, with the Irwin's strain energy release rate. In the same case, Γ has the meaning of the critical magnitude of the strain energy release rate.

For fatigue cracks, the generalized forces G and Γ depend not only on characteristic loads and crack dimensions, but also on the parameters characterizing microdamage at the crack tip. A fatigue crack does not propagate if

$$G < \Gamma, \tag{5}$$

and grows in a stable way, without jumps, if

$$G = \Gamma, \quad \frac{\partial G}{\partial a} < \frac{\partial \Gamma}{\partial a}. \tag{6}$$

If the second of conditions (6) is not fulfilled, it means that the crack propagates in a jump-like way, going from one sub-equilibrium (stable) state to the neighboring sub-equilibrium state. The sizes of jumps can be estimated from the energy balance considerations. However, since the sizes of jumps are small and the jump-like character of crack propagation is smoothed significantly due to the material local nonhomogeneities, one might assume that a crack grows almost continuously under the condition

$$G \approx \Gamma. \tag{7}$$

To close the set of equations governing the fatigue crack growth, one needs a model of microdamage accumulation along the crack trajectory, as well as a relationship between the generalized forces and microdamage parameters. Some of these equations can be substantiated with the use of experimental data, other ones might be considered as *ad hoc* hypotheses. Anyway, different assumptions are to be introduced for high-cycle and low-

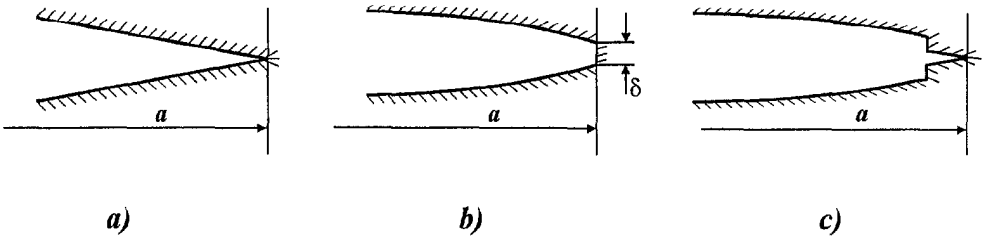

Fig. 1. Schematic presentation of the transition (a) from the high-cycle fatigue, (b) to the low-cycle fatigue, (c) and vice versa.

cycle fatigue cracks. Since the effects of overloading on the fatigue crack growth are born from plastic straining and related residual stresses, the joint consideration of high-cycle and low-cycle fatigue is needed to describe these effects. The transition from one type of fatigue to another is illustrated schematically in Fig. 1 where blunting of an initially sharp high-cycle fatigue crack due to plastic deformation and the following return to the high-cycle fatigue is shown.

2. MODEL OF HIGH-CYCLE FATIGUE

Consider an opening mode planar crack in the plain stress conditions (Fig. 2). The length of the crack is $2a$, and applied (remote) stress is $\sigma_\infty(t)$. Treating the cycle number N as a continuous variable, assume that the fatigue crack growth is governed by extremal magnitudes of $\sigma_\infty(t)$ during a loading cycle, or by its maximal magnitude denoted simply $\sigma_\infty(N)$ and the range within a cycle $\Delta\sigma_\infty(N)$. Along with the applied stress, the "true" opening stresses $\sigma_y(x, N)$ distributed at $|x| > a$, $y = 0$ are of interest. Their maximal magnitudes during a cycle and the range are denoted $\sigma_y(x, N)$ and $\Delta\sigma_y(x, N)$, respectively.

Let microdamage at $|x| \geqslant a$, $y = 0$ be described with the scalar measure $\omega(x, N)$ with magnitudes from the segment [0, 1]. At $\omega = 0$ the material is nondamaged and at $\omega = 1$ is completely damaged. Evidently, such a measure is similar to that introduced for creep damage by Rabotnov (1979) and Kachanov (1986). A rather universal model of microdamage accumulation is given with the equation

$$\frac{\partial\omega}{\partial N} = f(\Delta\sigma_y, r) \tag{8}$$

which right-hand side depends on the opening stress ratio $r = \sigma_y^{\min}/\sigma_y^{\max}$. Note the difference

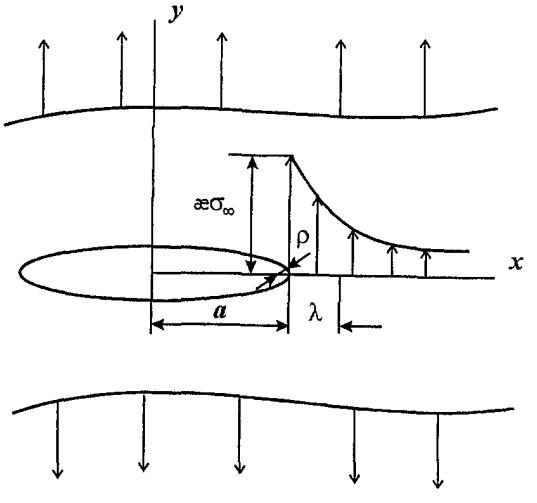

Fig. 2. Opening mode fatigue planar crack.

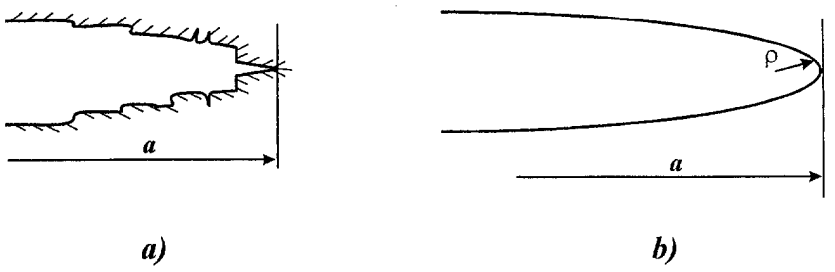

Fig. 3. Fatigue crack in a polycrystalline material and its schematization as an elliptical slit.

between r and the conventional stress ratio $R = \sigma_\infty^{\min}/\sigma_\infty^{\max}$ of extremal applied stresses within a cycle. Equation (8) can be specified as follows (Bolotin, 1983):

$$\frac{\partial\omega}{\partial N} = \left(\frac{\Delta\sigma_y - \Delta\sigma_{\text{th}}}{\sigma_\omega}\right)^m. \tag{9}$$

The parameters σ_ω, $\Delta\sigma_{\text{th}}$ and m characterize the resistance of the material to microdamage accumulation. Among them the characteristic stress σ_ω is of the order of magnitude of the "real" ultimate stress in tension, $\Delta\sigma_{\text{th}}$ is a threshold resistance stress that could depend on the local stress ratio r and, therefore, could take into account the crack closure and related phenomena. The exponent m is similar to the exponent entering in fatigue curves and fatigue crack growth rate diagrams and sometimes may coincide with those exponents. All the parameters, σ_ω, $\Delta\sigma_{\text{th}}$ and m, generally depend on temperature and other environmental conditions. If $\sigma_y < \Delta\sigma_{\text{th}}$, the right-hand side in eqn (9) must be put to zero.

Both the driving generalized force G and the resistance generalized force Γ that enter eqns (5)–(7), generally, depend on $\omega(x, N)$. For example, due to microdamage, the elastic moduli change in the vicinity of the crack tip resulting in the change of stress–strain field that, in its turn, affects the microdamage distribution near the tip (Bolotin and Kovekh, 1993). A more significant effect is the decreasing of the fracture toughness due to microdamage at the tip. This effect can be taken into account assuming that

$$\Gamma = \Gamma_0(1 - \psi^\varkappa). \tag{10}$$

Here Γ_0 is the generalized resistance force (namely, the specific fracture work) for the nondamaged material, $\psi(N)$ is the microdamage measure at the tip, i.e.

$$\psi(N) = \omega[a(N), N], \tag{11}$$

and the exponent $\varkappa > 0$, say, $\varkappa = 1$ (Bolotin, 1983).

To evaluate microdamage at the tip, we must reject from the common schematization of cracks as mathematical cuts. In fact, if a material is assumed linear elastic, the common model of linear fracture mechanics results in singularities of opening stresses at the crack tips. To avoid singularities, we treat fatigue cracks as narrow slits with finite curvature radii at the tip. A typical schematization is an elliptical slit with the larger semi-axis a and the tip curvature radius $\rho \ll a$. It does not mean at all that a crack has a smooth face surface. Moreover, the radius ρ or, precisely, the ratio ρ/a is just a measure of stress concentration near the tip of the crack that may have a rather complicated fractographic picture (Fig. 3).

In the earlier publications (Bolotin 1983, 1985) the effective tip radius was considered as a material parameter. Later this viewpoint was changed to take into account the tip blunting and sharpening during the crack growth. A crack blunts on overloading and sharpens when we return to the regular high-cycle fatigue (Fig. 1). Under other equal conditions, a crack sharpens at the stage of accelerated crack propagation and blunts when the microdamage accumulation process becomes a dominating phenomenon. To take into

account both tendencies, the simple differential equation with respect to $\rho(N)$ can be used such as:

$$\frac{\partial\rho}{\partial N} = \frac{\rho_s - \rho}{\lambda_\rho}\frac{da}{dN} + (\rho_b - \rho)\frac{d\psi}{dN}. \tag{12}$$

Here ρ_s is the "sharp" effective tip radius, ρ_b is the "blunt" effective tip radius and λ_ρ is a parameter with the dimension of length that characterizes the influence of crack growth rate da/dN on the sharpening process. The second term in the right-hand side of eqn (12) takes into account the tip blunting due to microdamage accumulation at the tip.

Assumption of the finite curvature at the tip allows one to introduce the bounded stress distribution along all the crack trajectory. If a crack length is small compared with the width of the specimen, the solution of the standard problem of elasticity theory (Timoshenko and Goodier, 1970) results in the following opening tensile stresses $\sigma_y(x, N)$ at $|x| \geq a$, $y = 0$:

$$\frac{\sigma_y}{\sigma_\infty} = \frac{\xi^2+\varepsilon}{\xi^2-\varepsilon} + \frac{(1-\varepsilon)^2}{2}\frac{\xi^4+3\xi^2+\varepsilon(\xi^2-1)}{(\xi^2-\varepsilon)^3},$$

$$\xi = \frac{(x/a)+[(x/a)^2-(1-\eta)]^{1/2}}{1+\eta^{1/2}},$$

$$\varepsilon = \frac{a-b}{a+b}, \quad \eta = \frac{\rho}{a}, \quad \rho = \frac{b^2}{a}. \tag{13}$$

Equation (13) may also be used as an approximation for a bounded width. Then we ought to interpret σ_∞ as the nominal stress in the cross section, at $y = 0$. At $x = a$ eqn (13) results in Neuber's equation for the maximal opening stress

$$\sigma_y(a) = \left[1 + 2\left(\frac{a}{\rho}\right)^{1/2}\right]\sigma_\infty. \tag{14}$$

Returning to eqns (5)–(7), we use the linear fracture mechanics equation for the driving generalized force, i.e.

$$G = \frac{K^2}{E} \tag{15}$$

with Young's modulus E and stress intensity factor K. Equation (15) means that the influence of microdamage on Young's modulus and the resulting redistribution of stresses around the tip may be neglected (Bolotin and Kovekh, 1993). Under certain *ad hoc* assumptions, eqns (7) and (9)–(14) can be reduced to an ordinary differential equation with respect to $a(N)$ which includes all three phases of crack propagation: the initial growth near the threshold, the Paris–Erdogan phase and the final accelerated growth till the final rupture (Bolotin, 1983, 1985, 1989).

3. MODEL OF LOW-CYCLE FATIGUE

The simplest model of nonlinear fracture mechanics is a model of planar crack in the linear elastic material with a thin tip plastic zone where the opening stress σ_0 is given. The latter is of the order of magnitude of the yield limit and in some cases coincides with it. Therefore, the problem of plasticity theory is reduced to a problem of elasticity theory with the stresses given on the crack faces $|x| < a$ and on the borders of the plastic zones

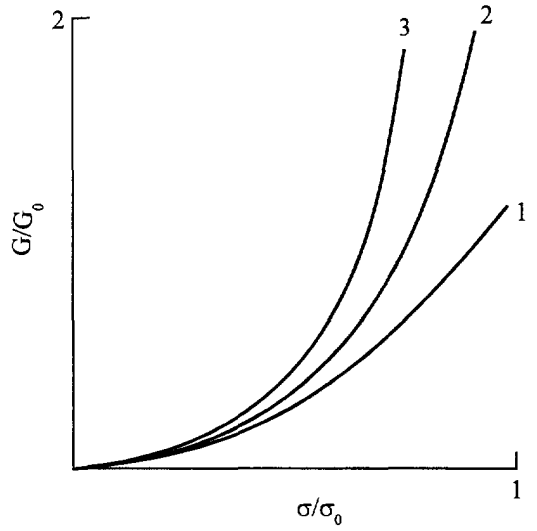

Fig. 4. Comparison of various approaches to evaluation of the generalized driving force: (1) linear elastic model, (2) J-integral; (3) present analysis.

$a \leqslant |x| \leqslant a+\lambda$. The size λ of the plastic zone is given with the equation (Liebowitz, 1968; Parton and Morozov, 1985; Pluvinage, 1989; Wnuk, 1990):

$$\lambda = a\left[\sec\left(\frac{\pi\sigma_\infty}{2\sigma_0}\right)-1\right], \tag{16}$$

where σ_∞ is the applied (remote) tensile stress. The crack tip opening displacement is

$$\delta = \frac{8\sigma_0 a}{\pi E}\ln\left[\sec\left(\frac{\pi\sigma_\infty}{2\sigma_0}\right)\right]. \tag{17}$$

Application of the common J-integral technique leads to the equation

$$J = \sigma_0\delta = \frac{8\sigma_0^2 a}{\pi E}\ln\left[\sec\left(\frac{\pi\sigma_\infty}{2\sigma_0}\right)\right]. \tag{18}$$

However, the J-integral cannot be considered as a generalized force in this problem. In fact, the product $J\delta a$ is not (opposite to the elastic case) a component of the virtual work. Using the general approach, we define the driving generalized force through the virtual work $\delta_G A_e$ of external and $\delta_G A_i$ of internal forces:

$$G \overset{\text{def}}{=} \frac{\delta_G A_e + \delta_G A_i}{\delta a}.$$

It means, compared with the J-integral technique, that the variation of the plastic zone length is also taken into account. Using eqns (16) and (17) we obtain

$$G = \frac{8\sigma_0^2 a}{\pi E}\left[\ln\cos\left(\frac{\pi\sigma_\infty}{2\sigma_0}\right)+\frac{\pi\sigma_\infty}{2\sigma_0}\operatorname{tg}\left(\frac{\pi\sigma_\infty}{2\sigma_0}\right)\right]. \tag{19}$$

The right-hand side coincides with the magnitude of "specific fracture work" estimated for the Leonov–Panasyuk–Dugdale model (Parton and Morozov, 1985).

The comparison of results delivered with eqns (15), (18) and (19) is presented in Fig. 4 (lines 1, 2 and 3, respectively). There, all G are normalized to $G_0 = 8\sigma_0^2 a/(\pi E)$. At

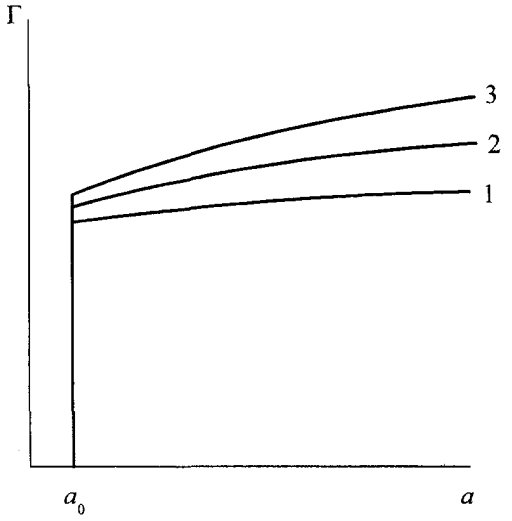

Fig. 5. Generalized resistance force as function of $a-a_0$ at three increasing applied stress levels 1, 2, 3.

$\sigma_0/\sigma_\infty \ll 1$ the discrepancy between the lines is small. But it could become significant in the area of low-cycle fatigue when σ_∞ is of the order of σ_0.

The generalized resistance force Γ depends not only on the microdamage measure ψ but also on the crack tip displacement δ:

$$\Gamma = \Gamma_0 f(\delta, \psi). \tag{20}$$

Here Γ_0 is the resistance force for the nondamaged material. As to the function $f(\delta, \psi)$, there is not sufficient information on it. When $\psi \equiv 0$, the force Γ, evidently, is similar to the resistance to ductile fracture usually associated with the so-called R-curve. According to widespread opinion, the force R plotted against the crack size a or its increment $a-a_0$ enters as a kind of a universal characteristic of the material resistance to ductile fracture. It is more sensible to assume that the resistance force R depends both on the size a and on the applied stress σ_∞. For example, one may consider it dependent on the crack tip opening displacement δ. Since, according to eqn (17), displacement δ is proportional to the crack size, the new assumption does not contradict the common interpretation of R-curves. But δ depend on σ_∞, too (see Fig. 5 where lines 1, 2, 3 are drawn for three increasing applied stress levels). At sufficiently small σ_∞/σ_0 eqn (17) results in

$$\delta \approx \frac{2\pi\sigma_\infty^2 a}{E\sigma_0}. \tag{21}$$

It means that not only the crack size, but also the level of applied stresses is responsible for the magnitude of the resistance force. Since G is growing with σ_∞ approximately in the same way as Γ, the σ_∞-dependence is not so significant in the general balance of forces.

In this paper we assume that the tip opening displacement and microdamage at the tip interact as follows:

$$\Gamma = \Gamma_0\left[1+\left(\frac{\delta-\delta_{th}}{\delta_f}\right)^\beta (1-\psi^\alpha)\right]. \tag{22}$$

Here δ_f, δ_{th}, α, and are materials parameters that, generally, depend on the interior structure of the cycle, say, on $r = \sigma_y^{min}/\sigma_y^{max}$. If $\delta \leqslant \delta_{th}$, instead of eqn (22) we have to use eqn (10). The inequality $\delta \leqslant \delta_{th}$ means that the plastic deformations at the tip stop playing the dominant role and only the influence of microdamage is to be taken into account. The following calculations include the solution of eqn (7) with account of eqns (19) and (22).

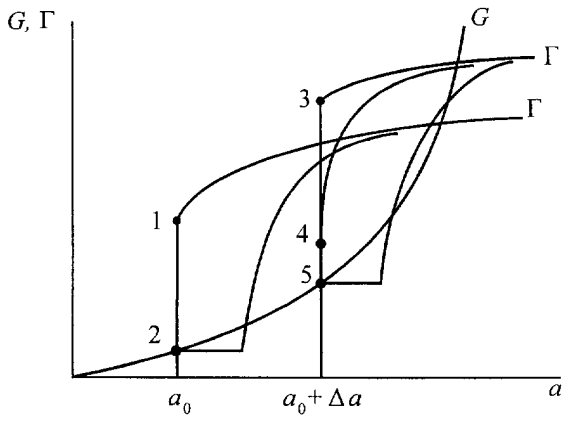

Fig. 6. Illustration to the computational procedure (explanation in the text).

The computational procedure is illustrated in Fig. 6 where the generalized forces G and Γ are plotted against the crack size a at various cycle numbers N. At $N = 0$, $a = a_0$, the inequality $G < \Gamma$ takes place (point 1). At $N > 0$ the process of microdamage accumulation proceeds resulting in the decrease of the resistance force Γ. This process terminates at $N = N_*$ when the equality $G = \Gamma$ is primarily attained (point 2). If a plastic zone exists near the crack tip, the attained state of equilibrium is unstable and it means a jump-like propagation of the crack up to $a_0 + \Delta a$. With the account of the microdamage accumulated before the jump, the initial resistance force (point 4) will be less than that for the non-damaged material (point 3). Then the process of the microdamage accumulation proceeds again until the equality $G = \Gamma$ is reached again (point 5). Since the jumps Δa are sufficiently small, the jump-like propagation can be approximated with a continuous one. In computation, it seems easier to treat Δa as given increments of the crack size and to evaluate the correspondent increments ΔN of the cycle number by the solution of eqn (7).

4. MICRODAMAGE WITH ACCOUNTED PLASTIC DEFORMATION

One of the central questions of the theory of the low-cycle fatigue is the choice of the model of microdamage accumulation. In principle, two different models can be considered. According to the first model, microdamage is produced with the cyclic stresses acting in the plastic zone and along its propagation. The second model connects the microdamage accumulation with the cyclic variation of strains within the plastic zone (Radon, 1990). A number of intermediate and mixed models can be suggested too, including those taking into account cyclic hardening and/or softening of the material, residual stress and strain fields, etc.

As in the high-cycle fatigue, we describe microdamage with the scalar measure $\omega(x, N)$ with magnitudes from segment [0,1]. When microdamage is stress-controlled, the equation of microdamage accumulation can be taken as similar to eqn (8). In an alternative case, one can assume instead of eqn (8) the following equation:

$$\frac{\partial \omega}{\partial N} = f_1(\Delta\varepsilon, r). \tag{23}$$

Here $\Delta\varepsilon$ is the range of strains (complete or purely plastic) within a cycle and r may be interpreted both as the stress or strain ratio. The choice between eqns (8) and (23) is to be done by comparing the numerically simulated results with experimental data. The preliminary analysis appears to be in favour of the stress-controlled model (Bolotin, 1989). At least, this model provides the exponent of the Paris–Erdogan part of the fatigue crack growth rate diagram rather close to two under very wide assumptions on the right-hand side of eqn (8).

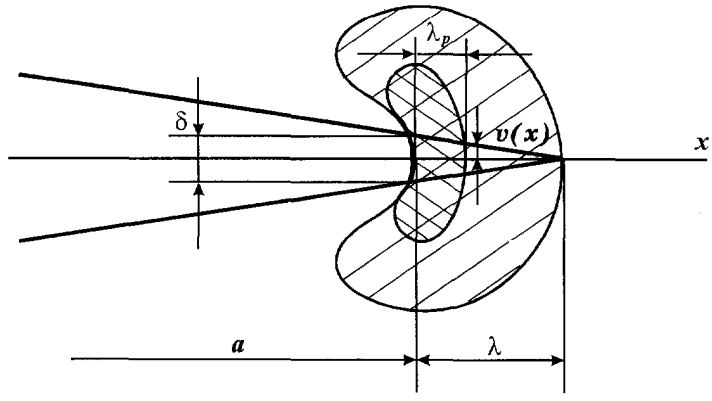

Fig. 7. Plastic zone at the crack tip for a single loading (dashed) and cyclic loading (double dashed).

In the framework of elastoplastic fatigue problems it is necessary to take into account the primary, i.e. corresponding to the loading half-cycle, stresses as well as secondary stresses such as residual ones. If the material is ideal elasto-plastic with the yield stresses $\pm\sigma_0$, a process zone of the size λ_p exists, and the stress range within it is equal to $2\sigma_0$ (Fig. 7). The size λ_p can be assessed from eqn (16) if we replace σ_0 with $2\sigma_0$, and σ_∞ with $(\sigma_\infty^{max}-\sigma_\infty^{min}) = \sigma_\infty(1-R)$. Here $\sigma_\infty \equiv \sigma_\infty^{max}$ and $R = \sigma_\infty^{min}/\sigma_\infty^{max}$ is the ratio of applied stresses. Then eqn (16) results in

$$\lambda_p = a\left[\sec\left(\frac{\pi\sigma_\infty(1-R_\infty)}{4\sigma_0}\right)-1\right]. \tag{24}$$

In particular, at $R = 0$ we obtain that $\lambda_p = \lambda/4$. The opening stress ranges at $y = 0$ are as follows:

$$\Delta\sigma_y(x) = \begin{cases} 2\sigma_0, & a \leqslant |x| \leqslant a+\lambda_p, \\ \dfrac{4\sigma_0}{\pi}\operatorname{arc\,ctg}\left\{\dfrac{a}{x}\left[\dfrac{x^2(a+\lambda_p)^{-2}-1}{1-a^2(a+\lambda_p)^{-2}}\right]^{1/2}\right\}, & |x| > a+\lambda_p, \end{cases} \tag{25}$$

and the residual stresses

$$\Delta\sigma_{res}(x) = \begin{cases} -\sigma_0, & a \leqslant |x| \leqslant a+\lambda_p, \\ \sigma_0 - \dfrac{4\sigma_0}{\pi}\operatorname{arc\,ctg}\left\{\dfrac{a}{x}\left[\dfrac{x^2(a+\lambda_p)^{-2}-1}{1-a^2(a+\lambda_p)^{-2}}\right]^{1/2}\right\}, & a+\lambda_p \leqslant |x| \leqslant a+\lambda, \\ \dfrac{2\sigma_0}{\pi}\operatorname{arc\,ctg}\left\{\dfrac{a}{x}\left[\dfrac{x^2(a+\lambda)^{-2}-1}{1-a^2(a+\lambda)^{-2}}\right]^{1/2}\right\} & \\ \quad -\dfrac{4\sigma_0}{\pi}\operatorname{arc\,ctg}\left\{\dfrac{a}{x}\left[\dfrac{x^2(a+\lambda_p)^{-2}-1}{1-a^2(a+\lambda_p)^{-2}}\right]^{1/2}\right\}, & |x| > a+\lambda. \end{cases} \tag{26}$$

It is assumed in eqn (26) that the mean stress $(\sigma_\infty^{max}+\sigma_\infty^{min})/2$ does not produce plastic deformations but σ_∞^{max} and $\sigma_\infty^{max}-\sigma_\infty^{min}$ do. That is typical, say, for the case $R = 0$. The stress

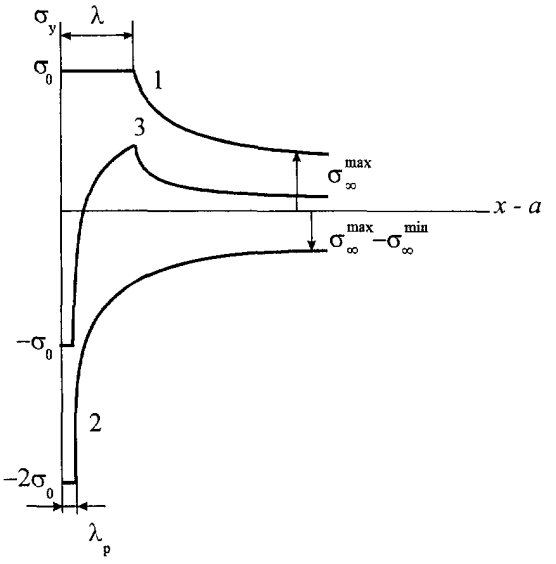

Fig. 8. Stress distribution ahead of crack: (1) loading half-cycle; (2) reverse loading; (3) residual stresses.

distribution ahead of the crack is illustrated in Fig. 8 where line 1 corresponds to the loading half-cycle, line 2 to the unloading with the range $\sigma_\infty^{\max} - \sigma_\infty^{\min}$ and line 3 to residual stresses.

In the further analysis, we use eqn (9) with material parameters σ_0, $\Delta\sigma_{\text{th}}$, m that, generally differ from the corresponding parameters of the high-cycle fatigue model. In particular, the threshold resistance stress $\Delta\sigma_{\text{th}}$ depends strongly on the residual stress σ_{res}. The simplest assumption is

$$\sigma_{\text{th}} = \Delta\sigma_{\text{th}}^0 - k\sigma_{\text{res}}, \tag{27}$$

where k is an empirical constant. At $\sigma_{\text{res}} < 0$ eqn (27) describes the increase of the threshold or, that is the same, the decrease of the effective stress range due to compression in the tip zone. Other parameters of eqn (9), generally, also depend on σ_{res}.

One of the questions arising in connection with the suggested models is the condition of transition from the high-cycle to the low-cycle fatigue and vice versa. It is obvious that eqn (19) transfers continuously into eqn (15) with decreasing of the applied stress level. Similarly, eqn (22) allows a continuous transition to eqn (10). As to eqns (13) and (25), (26) that describe the stress distribution along the prolongation of the crack, they are, from the analytical viewpoint, incompatible. A pragmatic way to find a bridge between them is to choose such a small zone of the plastic zone λ that at lesser λ we turn from the eqns (25), (26) to eqn (13) or to its equivalent. Actually, let $\rho \sim \lambda$ where λ is evaluated from eqn (16) as

$$\lambda \approx \frac{\pi^2 \sigma_\infty^2 a}{8\sigma_0^2}. \tag{28}$$

Then the elastic tip stress $\sigma_y(a)$ defined with eqn (14) is of the order of σ_0:

$$\sigma_y(a) \approx 2\sigma_\infty \left(\frac{a}{\lambda}\right)^{1/2} \approx \frac{4\sqrt{2}}{\pi}\sigma_0.$$

There are several parameters in the model of fatigue crack growth with the dimension of length. The most suitable candidate for the border length is the "blunt" effective tip

radius ρ_b from eqn (12). Later on, we assume that at $\lambda \geqslant \rho_b$ the high-cycle fatigue model and at $\lambda > \rho_b$ the low-cycle fatigue model is to be used.

5. HIGH-CYCLE FATIGUE WITH SINGLE OVERLOADINGS

Consider a regular cyclic loading interrupted with single overloadings (Fig. 8). Let the regular loading correspond to the high-cycle fatigue, but overloadings produce significant plastic deformations with the tip zone $\lambda > \rho_b$. During the cycle of overloading we apply the thin plastic zone model. The length of the tip zones are given in eqns (16) and (24), the stress range in eqn (25) and the residual stresses in eqn (26). We assume that the generalized resistance force is given in eqn (22). Moreover, we assume that along the whole plastic zone the resistance to crack growth is governed with the equation similar to eqn (22)

$$\Gamma = \Gamma_0 \left[1 + \left(\frac{2v - \delta_{th}}{\delta_\omega} \right)^\beta (1 - \omega^\alpha) \right]. \tag{29}$$

Here the double plastic displacement $2v(x, N)$ at $a \leqslant x \leqslant a + \lambda$, $y = \pm 0$ and the microdamage measure $\omega(x, N)$ ahead of the crack are introduced instead of δ and ψ, respectively. The displacement $v(x)$ is defined with the equation (Wnuk, 1990)

$$v(x) = \frac{(a+\lambda)\sigma_0}{\pi E} \left[\cos(\theta) \ln \frac{\sin^2(\beta - \theta)}{\sin^2(\beta + \theta)} + \cos(\beta) \ln \frac{(\sin\beta + \sin\theta)^2}{(\sin\beta - \sin\theta)^2} \right],$$

$$\theta = \arccos\left(\frac{x}{a+\lambda} \right), \quad \beta = \frac{\pi\sigma_\infty}{2\sigma_0}. \tag{30}$$

Together with eqn (27), the introduced assumptions take into account all the principal mechanisms entering into overloading phenomena: the increasing of the material resistance to crack growth due to the crack tip blunting and plastic deformations within the tip zone, the residual stresses on the prolongation of the crack affecting the lower threshold of microdamage accumulation. The last mechanism is illustrated in Fig. 9. There the variation of the opening tensile stresses $\sigma_y(a, N)$ at the moving crack tip are shown. Being stationary under regular cyclic loading, the opening tensile stress changes significantly during the overloading and immediately after it. After passing the tip zone with residual compressive stresses, the recovering of the stresses takes place until the next overloading.

The computation program is rather cumbersome and, in some details, sophisticated since it contains multiple switchings from one loading process to another. Some numerical results for a central crack are presented in Figs 10–14. The following input data are used. The loading process during the regular stage is taken with $\Delta\sigma_\infty = 5$ MPa, $R = 0$. At overloadings we assume that $\Delta\sigma_\infty = 50$ MPa, $R = 0$. Material parameters in the high-cycle fatigue are: $E = 200$ GPa, $\Gamma_0 = 15$ kJ m^{-2}, $\sigma_\omega = 5$ GPa, $\Delta\sigma_{th} = 0.5$ GPa, $m = 2$, $\alpha = 1$, $\rho_s = 50$ μm, $\rho_b = \lambda_p = 100$ μm. During the elasto-plastic stage the material parameters are: $\sigma_0 = 500$ MPa, $\delta_\omega = 20$ μm, $\delta_{th} = 0$, $\beta = 0.5$, $k = 0.15$. The width of the sheet is $b = 500$ mm, the initial crack half-length $a_0 = 30$ mm and the initial tip radius $\rho_0 = 0.3$ mm.

In Fig. 10 the crack size a is plotted against the cycle number N. Line 1 shows the crack growth under the regular loading ($\Delta\sigma_\infty = 5$ MPa). Line 2 corresponds to a single overloading after $N = 2.5 \times 10^6$ cycles with the subsequent return to the regular process. Line 3 is obtained for the case of two overloadings, at $N = 2.5 \times 10^6$ and $N = 5 \times 10^6$. The general pattern and the order of magnitude of the retardation stage are in agreement with experimental data (see, e.g. Cullen and Broek, 1987).

The crack growth rate da/dN after the retardation recovers practically to the same magnitude as before overloading (Fig. 11). The following figures show how the effective tip radius ρ (Fig. 12) and microdamage measure at the tip ψ (Fig. 13) vary during the crack propagation. Both the tip blunting and sharpening phenomena can be observed there. The

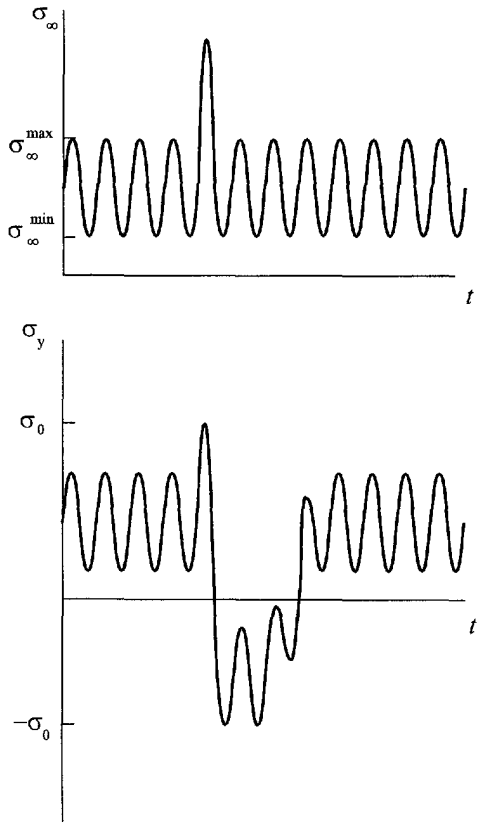

Fig. 9. Regular high-cycle fatigue loading with single overloadings and corresponding opening stresses.

blunting takes place when the crack is stationary or the propagation is relatively slowly. The sharpening is typical for the final stage when the effective tip radius tends to its "sharp" magnitude ρ_s. The tip microdamage measure ψ increases almost till the upper bound $\psi = 1$ when the crack propagates regularly and approaches the level accumulated in the far field at the final stage of crack growth.

The conventional crack growth rate diagram is shown in Fig. 14. Here the rate da/dN is plotted in the log–log scale against the range ΔK of the stress intensity factor K. Lines 1, 2, 3 are of the same meaning as in Fig. 10. The discontinuities correspond to the overloadings at $N = 2.5 \cdot 10^6$ and $N = 5 \cdot 10^6$. Both the threshold of crack growth and the acceleration

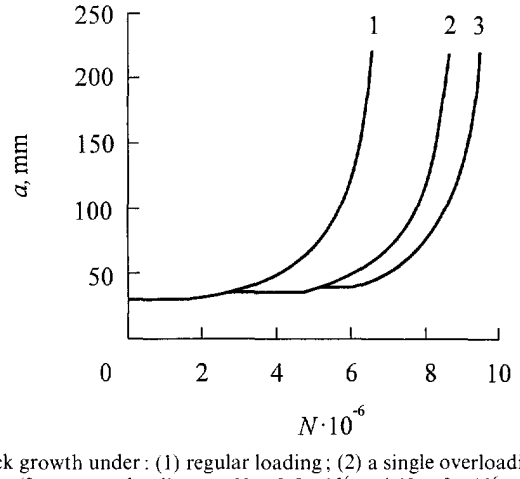

Fig. 10. Fatigue crack growth under: (1) regular loading; (2) a single overloading at $N = 2.5 \times 10^6$; (3) two overloadings at $N = 2.5 \times 10^6$ and $N = 5 \times 10^6$.

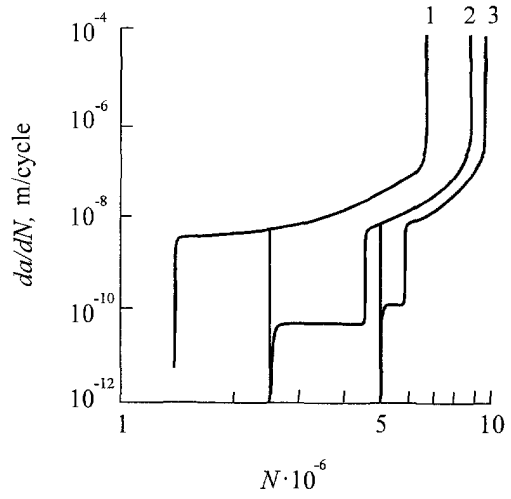

Fig. 11. Fatigue crack growth rate under: (1) regular loading; (2) a single overloading at $N = 2.5 \times 10^6$; (3) two overloadings at $N = 2.5 \times 10^6$ and $N = 5 \times 10^6$.

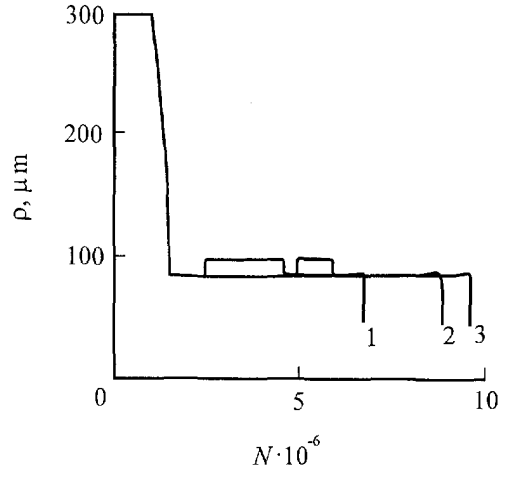

Fig. 12. Effective tip radius under: (1) regular loading; (2) a single overloading at $N = 2.5 \times 10^6$; (3) two overloadings at $N = 2.5 \times 10^6$ and $N = 5 \times 10^6$.

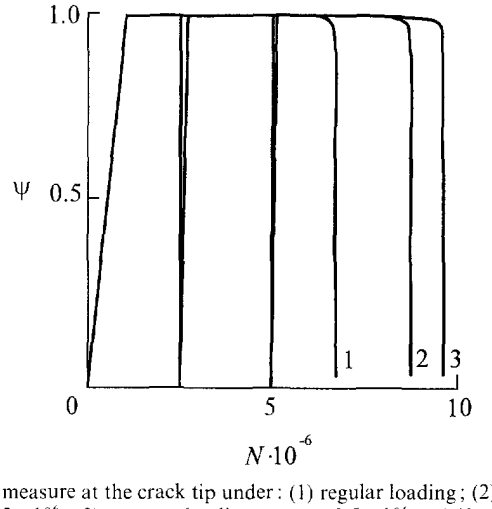

Fig. 13. Microdamage measure at the crack tip under: (1) regular loading; (2) a single overloading at $N = 2.5 \times 10^6$; (3) two overloadings at $N = 2.5 \times 10^6$ and $N = 5 \times 10^6$.

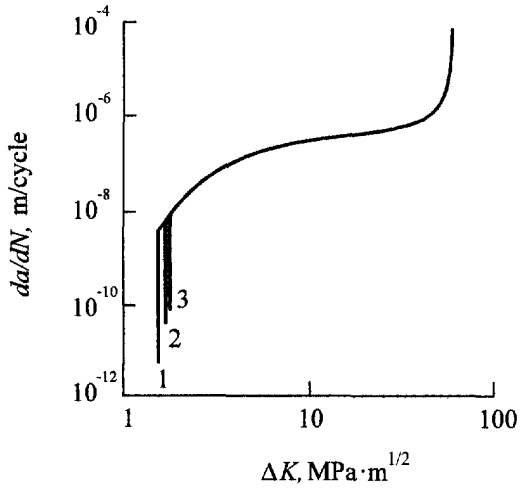

Fig. 14. Fatigue growth rate vs the range of stress intensity factor: (1) regular loading; (2) single overloading; (3) two overloadings.

during the final stage can be observed in Fig. 14 and this is in agreement with the general theory (Bolotin, 1989). After each retardation, the crack growth rate returns practically to the same magnitude, and the further paths of lines are nondistinguishable. It ought to be stressed that Fig. 14, as well as the preceding Figs 10–13, are plotted for the case of the identical initial crack size, $a_0 = 30$ mm. When the initial size of the crack is subjected to variation, a scattering of the crack growth rate lines takes place even under purely deterministic numerical data and regular loading (Bolotin *et al.*, 1994).

Acknowledgements—This work was supported by the Russian Foundation for Basic Research (grant no. 93-013-16486), and by the International Science Foundation (grant RLS000).

REFERENCES

Bolotin, V. V. (1983). Equations of fatigue crack growth. *Izv. Akad. Nauk SSSR, Mekh. Tverd. Tela* (*MTT*) **4,** 153–160 (in Russian).

Bolotin, V. V. (1985). A unified approach to damage accumulation and fatigue crack growth. *Engng Fracture Mech.* **22,** 387–398.

Bolotin, V. V. (1987). A model a fatigue crack with a tip zone. *Prikl. Mekh.* **23,** 73–87 (in Russian).

Bolotin, V. V. (1989). *Prediction of Service Life for Machines and Structures.* ASME Press, New York (translated from the Russian edition 1984).

Bolotin, V. V. (1990). Mechanics of fatigue fracture. In: *Nonlinear Fracture Mechanics* (Edited by M. P. Wnuk), CISM Course 314, pp. 1–60. Springer, New York.

Bolotin, V. V. and Kovekh, V. M. (1993). Numerical simulation of fatigue crack growth in medium with microdamage. *Izv. RAN, Mekh. Tverd. Tela* (*MTT*) **2,** 132–142 (in Russian).

Bolotin V. V., Chirkov, V. P. and Minakov, B. V. (1994). Influence of initial conditions on fatigue crack propagation. *Izv. RAN, Mekh. Tverd. Tela* (*MTT*) **2,** 73–76 (in Russian).

Cullen, W. H. and Broek, D. R. (1987). The effect of reactor-typical loading on fatigue crack growth of pressure vessel steell in PWR environments. In: *Trans. SMiRT* 9, Lausanne, Vol. F, 149–154.

Hutchinson, J. W. (1979). *Nonlinear Fracture Mechanics.* Technical University Denmark, Lyngby.

Kachanov, L. M. (1986). *Introduction in Continuum Damage Mechanics.* Martinus Nijhoff, Dordrecht.

Liebowitz, H. (Ed.) (1968). *Fracture. An Advanced Treatise,* Vol. 2. Academic Press, New York.

Parton, V. Z. and Morozov, E. M. (1985). *Mechanics of Elasto-Plastic Fracture.* Nauka, Moscow (in Russian).

Pluvinage, G. (1989). *Mecanique Elastoplastique de la Rupture.* Cepad, Toulouse (in French).

Rabotnov, Yu. N. (1979). *Mechanics of Deformable Solids.* Nauka, Moscow.

Radon, J. C. (1990). Elasto-plastic futigue crack growth: mathematical models and experimental evidence. In: *Nonlinear Fracture Mechanics* (Edited by M. P. Wnuk), CISM Course 314, pp. 229–292. Springer, New York.

Timoshenko, S. P. and Goodier, J. N. (1970). *Theory of Elasticity,* 3rd Edn. McGraw-Hill, New York.

Wnuk, M. P. (1990). *Mathematical Modelling of Nonlinear Phenomena in Fracture Mechanics. Nonlinear Fracture Mechanics* (Edited by M. P. Wnuk), CISM Course 314. Springer, New York.